Site-Specific, Platform-Based Conjugation Strategy for the Synthesis of Dual-Labeled Immunoconjugates for Bimodal PET/NIRF Imaging of HER2-Positive Tumors

Pierre Adumeau, René Raavé, Milou Boswinkel, Sandra Heskamp, Hans Wessels, Alain van Gool, Mathieu Moreau, Claire Bernhard, Laurène da Costa, Victor Goncalves, et al.

Site-specific, platform-based conjugation strategy for the synthesis of dual labeled immunoconjugates for bimodal PET/NIRF imaging of HER2-positive tumors

Pierre Adumeau[†]*, René Raavé[‡], Milou Boswinkel[‡], Sandra Heskamp[‡], Hans JCT Wessels[§], Alain J van Gool[§], Mathieu Moreau[†], Claire Bernhard[†], Laurène Da Costa[†], Victor Goncalves[†], Franck Denat[†]*

[†] Institut de Chimie Moléculaire de l'Université de Bourgogne, UMR 6302, CNRS, Université Bourgogne Franche-Comté, 9 Avenue Alain Savary, 21000 Dijon Dijon, France
[‡] Department of Medical Imaging, Radboud Institute for Molecular Life Sciences, Radboud university medical centre, Geert Grooteplein Zuid 28, 6525 GA Nijmegen, The Netherlands
[§] Translational Metabolic Laboratory, Department of Laboratory Medicine, Radboud university medical centre, Geert Grooteplein Zuid 10, 6525 GA Nijmegen, The Netherlands
Corresponding authors: Dr. Pierre Adumeau, 9 Avenue Alain Savary, 21000 Dijon, France, email: pierre.adumeau@u-bourgogne.fr, phone: +33 380 393 818; Pr. Franck Denat, 9 Avenue Alain Savary, 21000 Dijon, France, email: franck.denat@u-bourgogne.fr, phone: +33 380 396 115.

ABSTRACT
Because positron emission tomography (PET) and optical imaging are very complementary, the combination of these two imaging modalities is very enticing in the oncology field. Such bimodal imaging generally relies on imaging agents bearing two different imaging reporters. In the bioconjugation field, this is mainly performed by successive random conjugations of the two reporters on the protein vector, but these random conjugations can alter the vector properties. In this study, we aimed at abrogating the heterogeneity of the bimodal imaging immunoconjugate and mitigating the impact of multiple random. A trivalent platform bearing a DFO chelator for ^{89}Zr labeling, a NIR fluorophore – IRDye800CW – and a bioconjugation handle was synthesized. This bimodal probe was site-specifically grafted to trastuzumab via glycan engineering. This new bimodal immunoconjugate was then investigated in terms of radiochemistry, *in vitro* and *in vivo*, and compared to the clinically relevant random equivalent. *In vitro* and *in vivo*, our strategy provides several improvements over the current clinical standard. The combination of site-specific conjugation with the monomolecular platform reduced the heterogeneity of the final immunoconjugate, improved the resistance of the fluorophore toward radiobleaching and reduced the non-specific uptake in the spleen and liver compared to the standard random immunoconjugate. To conclude, the strategy developed is very promising for the synthesis of better defined dual labeled immunoconjugates, although there is still room for improvement. Importantly, this conjugation strategy is highly modular and could be used for the synthesis of a wide range of dual labeled immunoconjugates.

Keywords: Bimodal, PET-NIRF, site-specific, MOMIP, trastuzumab.

INTRODUCTION

Past studies have demonstrated the benefits of near-infrared fluorescence (NIRF) guided surgery on the survival rate of patient, by facilitating complete resection of the tumor tissue.[1] This imaging technique, however, is unsuited for preoperative imaging due to its low penetration depth (typically below 2 mm). On the other hand, nuclear imaging (Positron Emission Tomography – PET - and Single Photon Emission Computed Tomography - SPECT) are deep penetrating, allowing non-invasive whole-body imaging particularly suited for preoperative imaging, but has only low spatial resolution. Combining these two complementary imaging modalities into one single imaging agent is therefore very enticing, and such approach has been the focus of several reviews.[2–6] Indeed, by combining fluorescence and nuclear imaging in a single imaging agent, it would be possible to stage and locate the disease before surgery by using non-invasive nuclear imaging, allowing to choose the best course of action for the patient welfare, while fluorescence imaging could be used during surgery to precisely assess the tumor margins and detect possible metastases hardly visible to the naked eye, reducing the chances of relapse. This bimodal imaging strategy has been applied to antibodies which, thanks to their high specificity and high affinity for their molecular target, demonstrated to be successful vectors for both PET/SPECT and NIRF imaging.

With the exception of rare cases such as radiolabeled BODIPY fluorophores,[7,8] the vast majority of these PET/NIRF and SPECT/NIRF conjugates implies the grafting of the antibody with two different reporters, each dedicated to one imaging modality. It is also possible to use two different conjugates for bimodal imaging, each conjugate bearing one of the reporters, but this cocktail approach is not ideal as it requires regulatory agreements for the two different compounds. In addition, the nature of the conjugated cargo is known to alter the pharmacokinetics of the antibody, potentially yielding a cocktail of two conjugates with different pharmacokinetics.

The easiest way to obtain a bimodal immunoconjugate – an antibody bearing both reporters - is indisputably by successively performing two lysine-based conjugations with two amine-reactive cargo derivatives.[2,4–6,9] This simple strategy has been used extensively for the synthesis of various PET/NIRF and SPECT/NIRF immunoconjugates, some of them making it to the clinic.[10,11] However, the lysine-based conjugation has its limitations. Given the high number of accessible lysines on an immunoglobulin G (IgG), this type of conjugation is by definition random – both in terms of conjugation sites and of degree of conjugation – which translates in high heterogeneity of the final conjugates, and can potentially lead to a loss of affinity.[12] Admittedly, these adverse effects are exponentially increased by the two successive random conjugations used for the synthesis of these bimodal immunoconjugates.

Two different strategies have been used in the past to limit the deleterious effects of this sequential conjugation in the synthesis of PET-optical immunotracers.

One way to reduce these effects is to use monomolecular multimodal imaging probe (MOMIP) platforms. Such platform combines in a single molecule the two different reporters and a lysine-reactive moiety such as an isothiocyanate, which allows the grafting of both cargoes with one single conjugation.[13–21] Although this strategy gives a facile and efficient control over the reporters ratio and reduces the number of impacted lysines compared to double-random conjugation, it still has the inherent limitations of a random conjugation.

Another strategy consists of controlling the conjugation site of at least one of the cargoes by using site-specific conjugation methods.[22–24] Although performing one of the conjugation site-specifically allows to reduce the heterogeneity and immunoreactivity impairment compared to double random conjugation, still the other conjugation – a random conjugation - brings its share of adverse effects.

Only two occurrences of synthesis of nuclear-NIRF conjugate involving only site-specific conjugations can be found in the literature. In the first example, Houghton *et al.* exempted themselves of random conjugations by site-specifically engineering an anti-CA19.9 antibody to sport four azide moieties.[25] This azide-bearing antibody was then simultaneously coupled with the IRDye800CW NIR-fluorophore and a chelator for $^{89}Zr^{4+}$ – desferrioxamine (DFO) – via a strain-promoted alkyne-azide cycloaddition (SPAAC). Although this strategy yielded site-specific conjugates and allowed to control the average ratio of the two reporters, this ratio on individual conjugates was ruled by a stochastic distribution, bringing heterogeneity at some level as well. In a more recent example, Spycher *et al.* used the mTGase – an enzyme creating a peptide bond between lysine derivatives and glutamine – to site specifically append the anti-CD30 cAC10-IgG1 antibody with a trans-cyclooctyne (TCO) and an azide moiety on glutamine-297 and lysine-340, respectively.[26] The TCO/azide-bearing antibody was then coupled with tetrazine-bearing DOTAGA chelator and a DBCO-bearing fluorophore, via IEDDA and SPAAC respectively, giving the final site-specifically dual-labeled conjugate with a fully controlled structure. However, this strategy relied on the specific reactivity of lysine-340 of this particular antibody, and it is likely that other antibodies would have a different conjugation pattern.

As we aimed at obtaining better-defined bimodal imaging conjugates with optimal immunoreactivity, we developed a simple and modular conjugation method combining the two strategies – platform and site-specific conjugation. Indeed, these two strategies have very complementary downsides and advantages. The platform gives complete control over the reporters ratio, but the random conjugation necessary to its attachment to the protein brings its lot of detrimental impact on the biological properties. On the other hand, the site-specific conjugation allows for a perfectly controlled conjugation with a defined number of reporters at a specific location, but beside a few particular cases it is impossible to implement on two different payloads without introducing heterogeneity. Combining the two approaches give us the ideal system for the grafting of multiple payloads on a biological vector: controlled payloads ratio, conjugation site and degree of labeling. This translates into a perfect homogeneity of the obtained conjugate and avoids any impairment of the immunoreactivity. Although this combination of site-specific grafting and MOMIP has been used on a few simple proteins,[27,28] it has never been applied to full-length immunoglobulins. In the study at hand, we produced a PET/NIRF MOMIP compatible with site-specific conjugation, bearing the DFO chelator – for ^{89}Zr chelation – the NIR fluorophore IRDye800CW and a bicyclononyne (BCN) for SPAAC-based bioconjugation. This MOMIP was site-specifically grafted to an azide-bearing trastuzumab, and the behavior of this site-specific MOMIP conjugate was compared with the current clinical standard – the dual random conjugate. For the sake of comparison, conjugates bearing solely DFO or IRDye800CW were also synthesized via site-specific and random conjugation, and included to this study. We herein report the results of these comparisons, in terms of *in vitro* and *in vivo* behavior.

RESULTS AND DISCUSSION

Design, synthesis and characterization

The choice of the two reporters – radionuclide and NIR fluorophore – was dictated by their clinical relevance for antibody labeling. We have turned our attention toward IRDye800CW, a water-soluble near-infrared fluorophore used in plethora of clinical trials for the labeling of antibodies.[1] Indeed, this fluorophore absorbs and emits photons in the tissue transparency window (700-1200 nm), making it well suited for fluorescence-guided surgery. Zirconium-89 and its chelator DFO attracted our notice as this pair has taken a prominent place in immunoPET imaging in the last decades, thanks to the excellent match between the

radioactive half-life of ^{89}Zr (3.3 days) and IgGs biological circulation time, and the satisfactory – although improvable – stability of the DFO-Zr(IV) complex.[29]

Among the different strategies available for the site-specific modification of antibodies, glycan engineering is particularly interesting.[30] Indeed, this strategy does not require pre-translational or genetic engineering to produce a modified antibody, and can virtually be used on every native antibody produced by mammalian cells. In addition, it is possible, by using different enzymes for the glycan truncation, to obtain conjugates with either 2 or 4 conjugation sites, allowing to easily adapt the degree of labeling of the final conjugate. Admittedly, the main drawback of this technique is the price of the kits marketed for these antibody modifications.

The strategy used in this study was developed by SynAffix and relies on the trimming of the glycan chain by the EndoS enzyme at the chitobiose core.[31] The thus revealed *N*-acetylglucosamine is then grafted with an azide-bearing galactosamide derivative via a promiscuous mutant of the galactosyltransferase (GalT Y289L), yielding a modified antibody with two azide moieties, one on each heavy chain.

The first step of this study was the synthesis of a trivalent MOMIP bearing an IRDye800CW as NIRF reporter, a DFO for later chelation of ^{89}Zr, and the azide-reactive strained alkyne BCN for site-specific coupling with an azide-bearing antibody.

The strategy used for the design of this MOMIP relies on a lysine platform, which has been successfully used in the past for the synthesis of trivalent platform.[13,14,32–34] Indeed, the lysine amino acid is an ideal scaffold for the synthesis of such trivalent platforms, as several lysines with orthogonal protecting groups are marketed for peptide synthesis and are easily accessible at affordable prices. The orthogonality of the different protecting groups thus allows for the sequential and selective amide couplings and deprotections to yield the final products in reasonable yield.

The PET/NIRF MOMIP **4** was obtained via a synthetic route of 4 steps, with a global yield of nearly 30% (fig. 1). First, the acid function of N-α-Fmoc-N-ε-Dde-L-lysine was coupled with DFO after in situ formation of the NHS ester derivative. The Dde protection of compound **1** was then cleaved in orthogonal conditions, freeing the ε-amine for reaction with an active carbonate of BCN. After cleavage of the Fmoc protective group to release the α-amine (compound **3**), an amide coupling was performed with IRDye800CW NHS-ester, yielding the final MOMIP Lys-BCN-DFO-IR800 **4**.

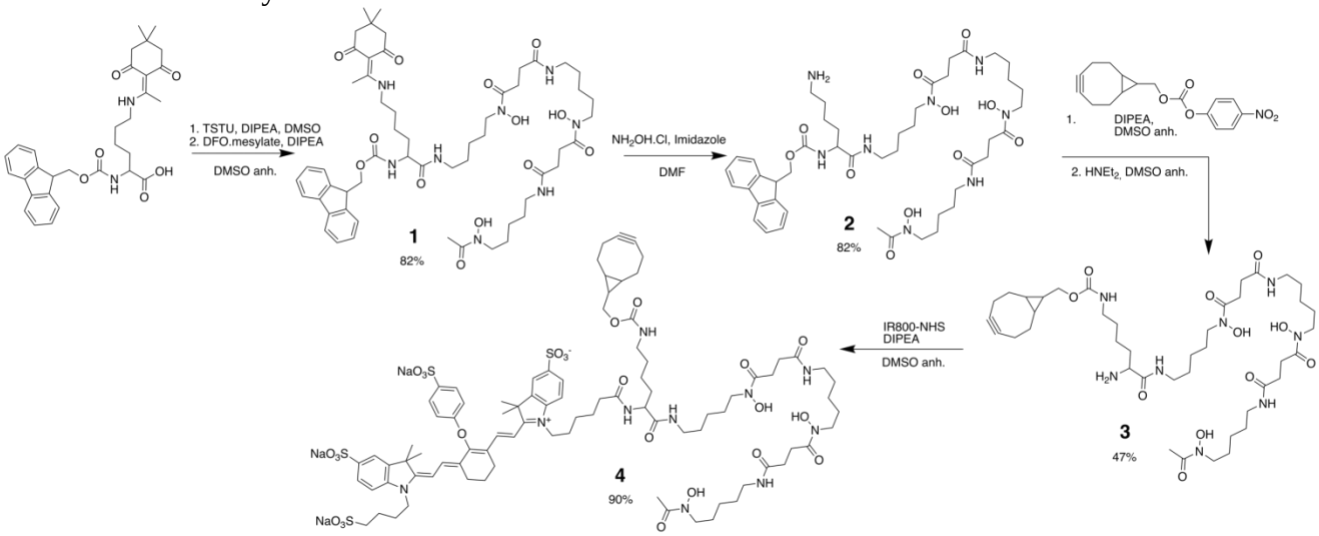

Figure 1. Synthesis of the trivalent MOMIP Lys-BCN-DFO-IR800 (4) using a lysine scaffold

As a proof of concept, a PET/NIRF conjugate was obtained by applying our approach to the trastuzumab antibody, a well-studied anti-HER2 antibody which has been extensively used in the past and is known for its robustness.

Native trastuzumab was first modified by enzymatic glycoengineering to site-specifically introduce two azide moieties per antibody (fig. 2). The BCN-bearing MOMIP was then coupled to these azide functions via a SPAAC reaction – strain promoted azide-alkyne cycloaddition - to give the site-specifically dual-labeled conjugate trast-^{ss}(DFO/IR800), with a theoretical maximum degree of labeling (DOL) of 2 for both chelator and fluorophore. MALDI-TOF and UV-vis spectrometry revealed DOL of 1.5 ± 0.3 and 1.7 ± 0.1 MOMIP per antibody, respectively (table S1), admittedly below the theoretical two MOMIP/mAb. The most likely cause of this suboptimal conjugation is the steric hindrance of the bulky MOMIP decreasing the reaction rate.

This site-specific MOMIP conjugate was compared with its random equivalent, obtained by successively performing two random conjugations with the amine-reactive DFO-isothiocyanate and IRDye800CW NHS-ester. Yet for the sake of comparison, random and site-specific DFO-bearing trastuzumab conjugates were also produced, as well as random and site-specific IR800-bearing trastuzumab conjugates (fig. 2). A particular attention was given to the DOL of the three random conjugates, in order to approach similar values as with the corresponding site-specific conjugates (table S1). As expected, this proved to be significantly difficult for the double random conjugation, where the random component of the two successive conjugations was even harder to tame and required a substantial amount of optimization.

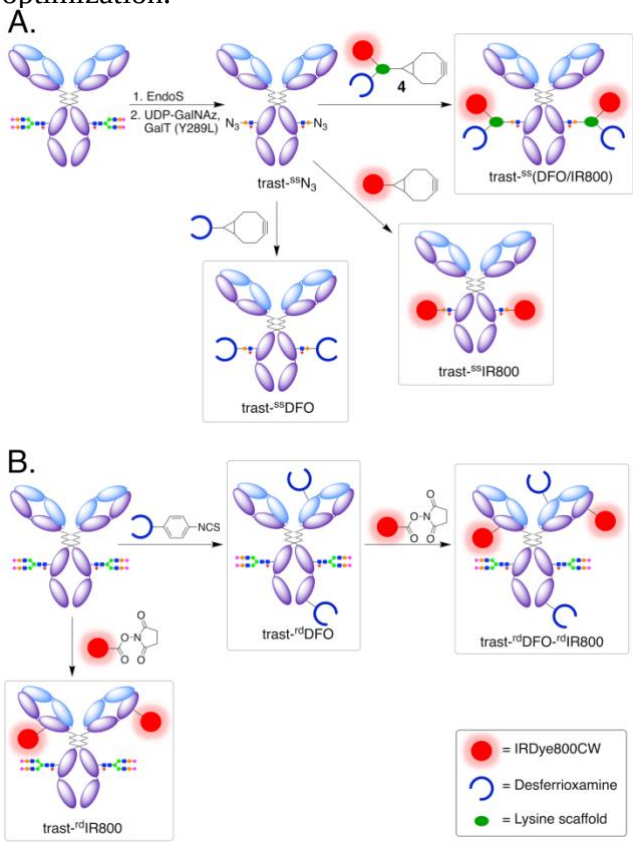

Figure 2. Synthesis of the site-specific MOMIP conjugate trast-^{ss}(DFO/IR800) and the site-specific DFO and IRDye800CW conjugates – trast-^{ss}DFO and trast-^{ss}IR800 – (A), and the standard random equivalents – trast-rdDFO-rdIR800, trast-rdDFO and trast-rdIR800 (B). For

clarity, only one example of the many possible structures of the random conjugates were cartooned

Mass spectrometry analysis of the conjugates

Detailed mass spectrometry characterization of trastuzumab conjugates – intermediates and end-products – was performed by liquid chromatography – mass spectrometry middle-down analyses of enzymatic FabRICATOR cleavage products Fc/2 (C-terminus half of the heavy chain), Fd' (N-terminus half of the heavy chain) and LC (light chain) fragments (fig. 3).

Analysis of the random IRDye800CW conjugate fragments showed mostly single IRDye800CW labeling on all three ~25 kDa fragments and minor double IRDye800CW labeling for the Fc/2 and Fd' fragments. Since *N*-glycans were still present on the Fc/2 fragment of random conjugates, this led to the detection of heterogenous Fc/2 forms consisting of unlabeled Fc/2 with the four dominant native glycoforms, four Fc/2 glycoforms modified with one IRDye800CW, and three very low abundance glycoforms bearing two IRDye800CW.

In contrast, trast-^{ss}IR800 and trast-^{ss}(DFO/IR800) conjugates were detected as only 2 dominant glycoforms of the Fc/2 fragment bearing single labels that respectively differed by the presence of a core fucose at the proximal *N*-acetylglucosamine residue. The site-specific conjugation was achieved at absolute specificity – no modification was detected on the Fd' and LC fragments – and with high yields of about 90% labeled end product, as shown by the analyses results of the EndoS-treated and azide-bearing intermediate (fig. S1) and site-specific conjugates.

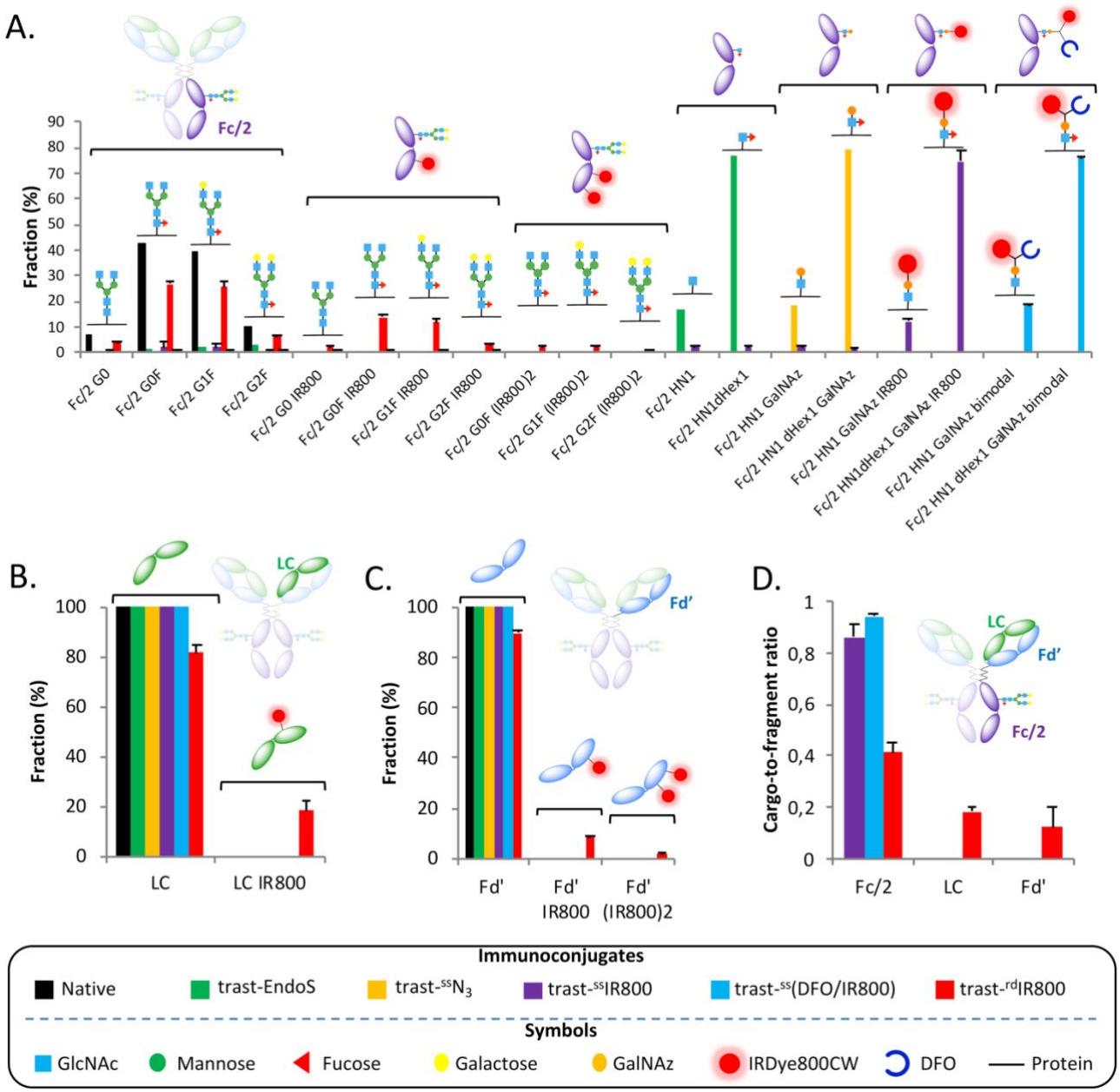

Figure 3. LC-MS middle-down characterization of intermediate and final conjugates for the (A) Fc/2, (B) LC, and (C) Fd' FabRICATOR fragments of trastuzumab conjugates. (D) Cargo to antibody-fragment ratio for the Fc/2, Fd' and LC frangments of trast-^{ss}IR800, trast-^{ss}(DFO/IR800) and trast-rdIR800. Legend: Native, native trastuzumab (n=1); trast-EndoS, EndoS-treated trastuzumab (n=1); trast-$^{ss}N_3$, N-azidoacetylgalactosamine-ligated EndoS-treated trastuzumab (n=1); trat-^{ss}IR800, site-specific IRDye800CW-trastuzumab conjugate (n=3); trast-^{ss}(DFO/IR800), site-specific MOMIP-trastuzumab conjugate (n=3); trast-rdIR800: random IRDye800CW-trastuzumab conjugate (n=3)

Taken together, these results show that the site-specific conjugation strategy applied to both IRDye800CW and the MOMIP is a highly efficient synthesis yielding considerably more uniform trastuzumab conjugate species compared to random conjugation, which produced heterogenous conjugate compositions with non-defined labeling positions at significantly lower labeling efficiency.

In vitro binding

All six conjugates displayed half-maximal inhibitory concentration (IC_{50}) values in the same nanomolar range, indicating that the conjugation strategy and the nature of the cargoes had only minimal consequences on the HER2-binding ability of the conjugates (fig. S2). These results are consistent with the known sturdiness of trastuzumab and previously reported observations, where even trastuzumab-DFO conjugates with dramatically high DOLs (up to 10 DFOs/mAb) retained an excellent immunoreactivity in the nanomolar range.[35]

Radiolabeling

The DFO-bearing conjugates – trast-rdDFO, trast-^{ss}DFO, trast-rdDFO-rdIR800, trast-^{ss}(DFO/IR800) – were radiolabeled with zirconium-89 using standard procedures (see SI). While good specific activities (A_s) and radiolabeling yield were obtained for trast-rdDFO, trast-^{ss}DFO and trast-rdDFO-rdIR800, the radiolabeling of the site-specific bimodal construct proved to be more difficult (table 1). Efforts at understanding this phenomenon are currently underway, though at present we hypothesize that this could be due to the structure and location of the MOMIP: the presence of the large fluorophore in the direct vicinity of the DFO, all located on a platform entangled between the two heavy chains, might be causing a steric hindrance limiting the access of Zr^{4+} to DFO or destabilizing the complex by preventing its optimal coordination geometry, but this will require confirmation by further investigation.

Table 1. ^{89}Zr-labeling efficiency for the DFO-bearing conjugates. Chelation rates were measured by iTLC of the crude mixture after 1h at 25°C

	Chelation rate (%)	RCY (%)	A_s (MBq/mg)
trast-^{ss}(DFO/IR800)	73.3 ± 11.5	72.7 ± 3.5	48.5 ± 2.1
trast-^{ss}DFO	98.7 ± 0.6	89.6 ± 2.1	54.7 ± 0.6
trast-rdDFO-rdIR800	93.3 ± 5.5	86.3 ± 2.1	55.7 ± 5.5
trast-rdDFO	97.3 ± 2.5	89.7 ± 5.5	56.3 ± 7.8

Stability studies

We then aimed at studying the behaviors of the different radioconjugates (fig. S3). In the presence of EDTA and DFO excess, both competing for the chelation of $^{89}Zr^{4+}$ with the DFO-grafted antibodies, the four radiolabeled immunoconjugates displayed very similar behaviors, showing no significant effect of the conjugation strategy over the stability of the Zr^{4+} chelates toward transchelation. However, the four conjugates exhibited slightly different stability in human plasma (fig. S3C). While [^{89}Zr]Zr-trast-rdDFO-rdIR800, [^{89}Zr]Zr-trast-^{ss}DFO and [^{89}Zr]Zr-trast-rdDFO remained fairly intact after 7 days at 37°C (93.6 ± 1.4 %, 96.8 ± 0.5 % and 95.4 ± 0.6 %, respectively), the site-specific bimodal construct [^{89}Zr]Zr-trast-^{ss}(DFO/IR800) released about 10% of its ^{89}Zr (88.1 ± 1.3 %), although this behavior was not significantly different from [^{89}Zr]Zr-trast-rdDFO-rdIR800. This intriguing lower stability in human plasma has yet to be explained, as it does likely not stem from a compromised stability of the zirconium chelate (see fig. S3A and S3B).

Fluorescence stability

A previous study by Hernandez and coworkers demonstrated that IRDye800CW and other cyanine-7 dyes were particularly sensitive to radiobleaching, a radiation-induced degradation of the fluorophore causing a gradual loss of fluorescence.[36] In light of this previous study, we set out to investigate the effect of the conjugation strategy on the fluorophore stability in presence of ^{89}Zr (fig. 4).

Very different photostabilities were observed for the site-specific and random bimodal constructs. After 7 days at 37°C in PBS, [^{89}Zr]Zr-trast-^{ss}(DFO/IR800) displayed almost no loss of fluorescence intensity - retaining 93 ± 10 % of the initial fluorescence intensity - while

the fluorescence of the random conjugate [^{89}Zr]Zr-trast-rdDFO-rdIR800 dropped to 25 ± 3 % of the initial fluorescence intensity (fig. 4A). In presence of ascorbic acid at 5.0 g/L, this decrease of fluorescence was not observed, confirming that this bleaching was induced by oxidative species, most likely species generated by radiolysis (fig. 4B). This radiobleaching was also observed in human plasma, although to a lesser extent due to the antioxidative properties of plasma (fig. 4C).[37]

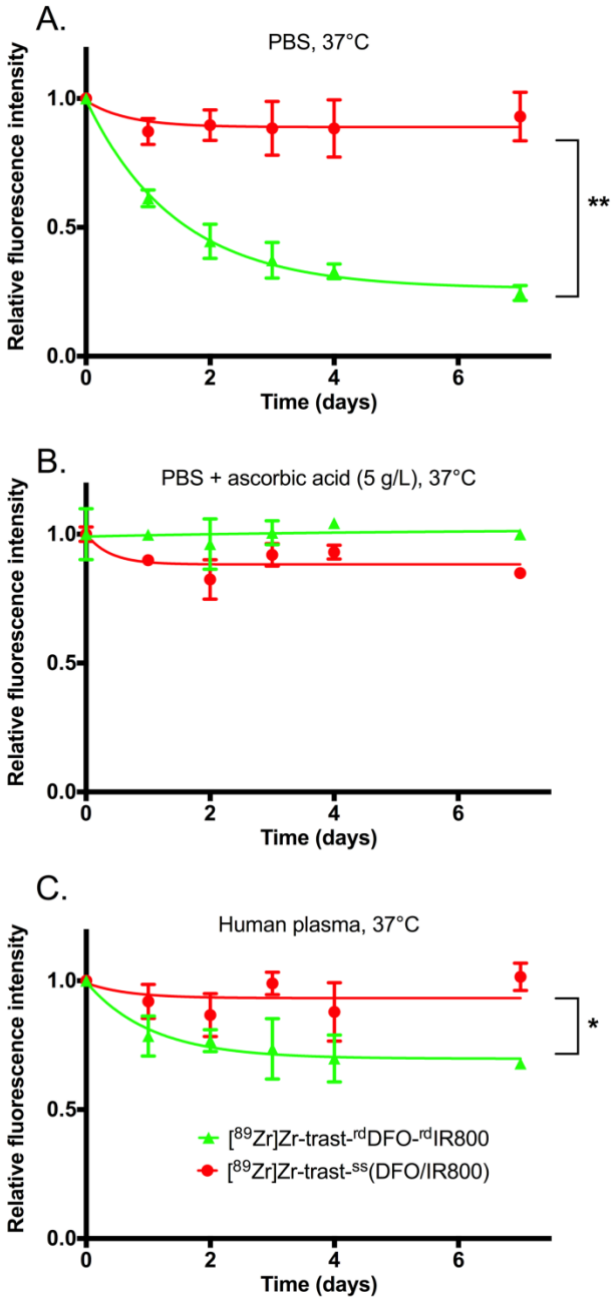

Figure 4. Fluorescence stability of [^{89}Zr]Zr-trast-rdDFO-rdIR800 and [^{89}Zr]Zr-trast-^{ss}(DFO/IR800) over 7 days in PBS (A), PBS supplemented with 5 g/L of ascorbic acid (B) and human plasma (C), at 37°C. Error bars represent standard deviations (n =3). *p < 0.05, **p < 0.01

In order to identify the protective mechanism at play on the site-specific bimodal conjugate, three "hybrid" bimodal conjugates combining random conjugation with site-specific conjugation and MOMIP were synthesized: trast-rdDFO-^{ss}IR800, trast-^{ss}DFO-rdIR800 and trast-rd(DFO/IR800) (fig. S4A, DOLs are presented in table S1). These conjugates were then radiolabeled and compared with the original [^{89}Zr]Zr-trast-^{ss}(DFO/IR800) and [^{89}Zr]Zr-trast-rdDFO-rdIR800, leading to the observation of two different trends (fig. S4B). The fluorescence of [^{89}Zr]Zr-trast-rdDFO-rdIR800, [^{89}Zr]Zr-trast-^{ss}DFO-rdIR800 and [^{89}Zr]Zr-trast-rd(DFO/IR800) decreased over 7 days in PBS, ultimately reaching less than 40% of their initial fluorescence (25 ± 3, 36 ± 2 and 29 ± 4 %, respectively). On the other hand, the fluorescence of [^{89}Zr]Zr-trast-^{ss}(DFO-IR800) and [^{89}Zr]Zr-trast-rdDFO-^{ss}IR800 remained much more stable over time, reaching 88 ± 1 and 83 ± 2 % of their initial fluorescence after 4 days, respectively. Interestingly, the behavior of [^{89}Zr]Zr-trast-^{ss}(DFO/IR800) and [^{89}Zr]Zr-trast-rdDFO-^{ss}IR800 slightly diverged after 7 days, although this was not significant. These differences in radio-bleaching behaviors between the various radioconjugates clearly indicate that the protective effect observed for [^{89}Zr]Zr-trast-^{ss}(DFO/IR800) was not due to the presence of the platform, the glycan truncation nor the site-specific grafting of the DFO chelator, but to the site-specific conjugation of the fluorophore, either alone or as part of the MOMIP.

Hence, this increased stability of the fluorophore could be explained by the steric hindrance of the heavy chains in the direct vicinity of the latter, reducing the accessibility of radicals and other radiolysis-generated reactive species to the fluorophore.

As expected, the non-radiolabeled conjugates trast-^{ss}IR800 and trast-rdIR800 showed no difference of behavior, both in PBS and human plasma (fig. S5).

In vivo PET imaging and *ex vivo* biodistribution

The blood kinetics were measured for the four radioconjugates and displayed very similar behaviors, suggesting that the conjugation methods and cargoes likely did not strongly impact the general perfusion rate in the overall organs nor the elimination rate (fig. S6).

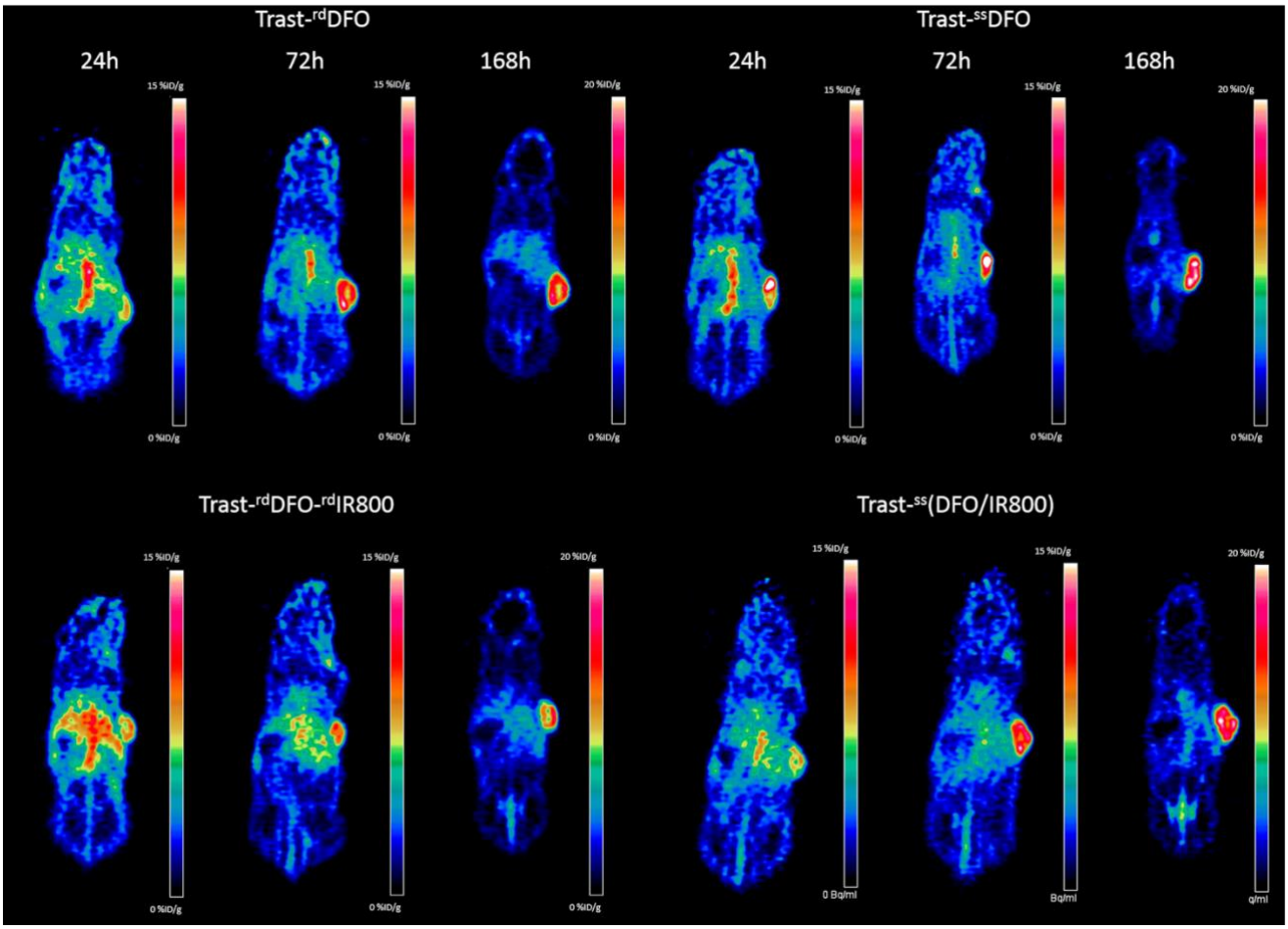

Figure 5. PET images (tumor-crossing coronal slice) of mice xenografted with HER2+ SKOV-3 cells, after injection of 1-5 MBq of [^{89}Zr]Zr-trast-rdDFO, [^{89}Zr]Zr-trast-^{ss}DFO, [^{89}Zr]Zr-trast-rdDFO-rdIR800, [^{89}Zr]Zr-trast-^{ss}(DFO/IR800). Scaling is corrected for injected dose and acqusition time. For each conjugate the same mouse is depicted at the different time points

The four radioconjugates allowed for a clear delineation of the tumor by PET, the activity building up in the tumor over the course of the experiment and yielding a high contrast with the background at 168 h post-injection (fig. 5 and fig. S7). As expected with radiolabeled antibodies, early timepoints yielded high background due to the high activity concentration in the blood pool. Uptake of radionuclide in bone was also visible for the four conjugates, and the presence of the fluorophore clearly increased the accumulation of activity in the liver compared to the DFO-only conjugates, both for the random and the site-specific radioconjugates.

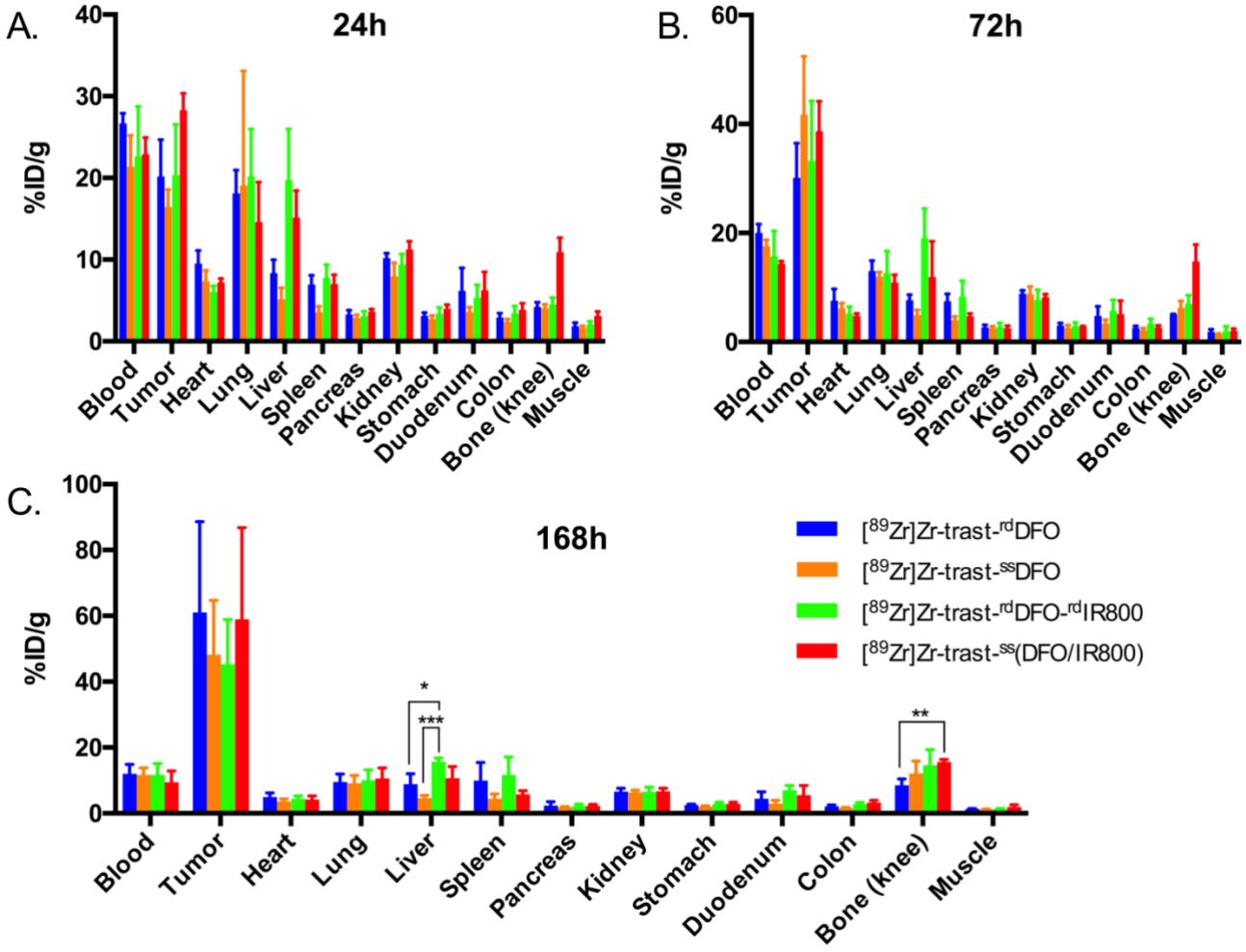

Figure 6. Ex-vivo biodistribution of [^{89}Zr]Zr-trast-rdDFO (blue), [^{89}Zr]Zr-trast-^{ss}DFO (orange), [^{89}Zr]Zr-trast-rdDFO-rdIR800 (green), [^{89}Zr]Zr-trast-^{ss}(DFO/IR800) (red) in HER2+ SKOV-3 tumor-bearing mice at 24 h (A), 72 h (B) and 168 h (C) after IV injection. Bars represent means with standard deviations (n=5). *p < 0.05, **p < 0.01, ***p < 0.001

The ex vivo biodistribution of the four radioconjugates gave a very similar result to PET imaging (fig. 6 and table S3). The tumor uptake of the four conjugates was comparable, increasing over time to reach about 50 %ID/g at 168 h post-injection. The random conjugates displayed a higher liver uptake than the site-specific conjugates (at 168 h p.i., 10.7 ± 3.6 and 15 ±1.0 %ID/g for [^{89}Zr]Zr-trast-^{ss}(DFO/IR800) and [^{89}Zr]Zr-trast-rdDFO-rdIR800, respectively; 4.7 ± 0.8 and 8.9 ± 3.1 %ID/g for [^{89}Zr]Zr-trast-^{ss}DFO and [^{89}Zr]Zr-trast-rdDFO, respectively) and, although not significantly different, in the spleen (5.8 ± 1.1 and 11.7 ± 5.4 %ID/g for [^{89}Zr]Zr-trast-^{ss}(DFO/IR800) and [^{89}Zr]Zr-trast-rdDFO-rdIR800, respectively; 4.5 ± 1.4 and 9.9 ± 5.6 %ID/g for [^{89}Zr]Zr-trast-^{ss}DFO and [^{89}Zr]Zr-trast-rdDFO, respectively). These observations are consistent with previous studies performed with radio immunoconjugates obtained through the same site-specific conjugation strategy, where lower accumulation in the liver and spleen were observed.[38,39] Indeed, the ablation - and to a lesser extend the truncation - of the Fc-glycans causes a conformational change of the Fc region of the antibody, which has been linked to a reduced interaction with FcγRI, a receptor on immune cells responsible for the sequestration of IgG1 in liver and spleen. Interestingly, no significant difference in the spleen uptake was observed between the two site-specific radioconjugates or the two random radioconjugates, indicating that the addition of the fluorophore – even on the glycan chain – likely did not alter the interaction with this receptor.

As could be expected, the presence of the fluorophore IRDye800CW on the bimodal constructs caused a dramatic increase of the liver uptake, nearly doubling the activity concentration both for the site-specific radioconjugate (10.7 ± 3.6 and 4.7 ± 0.8 %ID/g for [^{89}Zr]Zr-trast-^{ss}(DFO/IR800) and [^{89}Zr]Zr-trast-^{ss}DFO, respectively) and the random radioconjugate (15.7 ± 1.0 and 8.9 ± 3.1 %ID/g for [^{89}Zr]Zr-trast-rdDFO-rdIR800 and [^{89}Zr]Zr-trast-rdDFO, respectively). This has been correlated in previous studies with the increased lipophilicity of the conjugate caused by the fluorophore.[40–42] However, our site-specific MOMIP allows to reduce the impact of this fluorophore conjugation by nearly a third compared to the traditional dual random conjugation, reducing this activity uptake in the liver to levels comparable with the ones observed for the DFO-only random radioconjugate [^{89}Zr]Zr-trast-rdDFO.

The behavior of the four conjugates also differs in terms of bone uptake. At 24 h after injection, [^{89}Zr]Zr-trast-^{ss}DFO, [^{89}Zr]Zr-trast-rdDFO and [^{89}Zr]Zr-trast-rdDFO-rdIR800 display similar ^{89}Zr accumulation in bone (about 4 %ID/g on average) while a higher bone uptake is observed for the site-specific bimodal conjugate (up to 10%ID/g for the knee). The trend gradually fades over time to become less significant at 168 h post injection. This higher bone uptake of ^{89}Zr is likely to be related to the slight decrease of stability observed upon incubation in human serum (see above), but the precise cause of this suboptimal stability has yet to be elucidated. As for the remaining organs, the four radioconjugates exhibit similar uptakes, slowly clearing up over the course of the experiment.

In vivo NIRF imaging

The behavior of the bimodal conjugates was compared via NIR-fluorescence imaging to IRDye800CW-only trastuzumab conjugates (fig. S8). Semi-quantitative data were extracted from the fluorescence imaging (fig. S9). As expected, the general fluorescence intensity in the body decreased over time for the four immunoconjugates as they slowly left the blood circulation to accumulate into the tumor. Although substantial variations within time-points prevented us from drawing compelling conclusions, it appeared that in the case of the two random conjugates (trast-rdDFO-rdIR800 and trast-rdIR800) the fluorescence intensity at the tumor site decreased after 72 h, while this fluorescence intensity kept increasing for the two site-specific conjugates (trast-^{ss}(DFO/IR800) and trast-^{ss}IR800) over the studied timeframe (168 h). This apparent loss of fluorescence could be due to an increased degradation of the randomly-grafted dye upon internalization of the conjugate, but this point needs to be further investigated before drawing definitive conclusions. In spite of this fluorescence decline for the two random conjugates, the decrease over time of the general fluorescence in the body allowed to maintain excellent tumor-to body fluorescence ratios for all fluorescent conjugates (fig. S10). Yet, while the two bimodal conjugates displayed no significant difference in tumor-to-body ratios (3.6 ± 0.6 and 4.0 ± 1.2 for the random and site-specific conjugates, respectively), trast-rdIR800 and trast-^{ss}IR800 seemed to have significantly different behaviors, with the site-specific conjugate showing at 168 h p.i. a much higher tumor-to-body ratio (5.8 ± 0.9) compared to its random counterpart (2.4 ± 0.3). Importantly, all the tumor-to-body fluorescence ratios were of sufficient quality to successfully discriminate normal tissue from tumor tissue, and NIRF imaging was used to perform post-mortem fluorescence-guided tumorectomies with the four conjugate (fig.7).

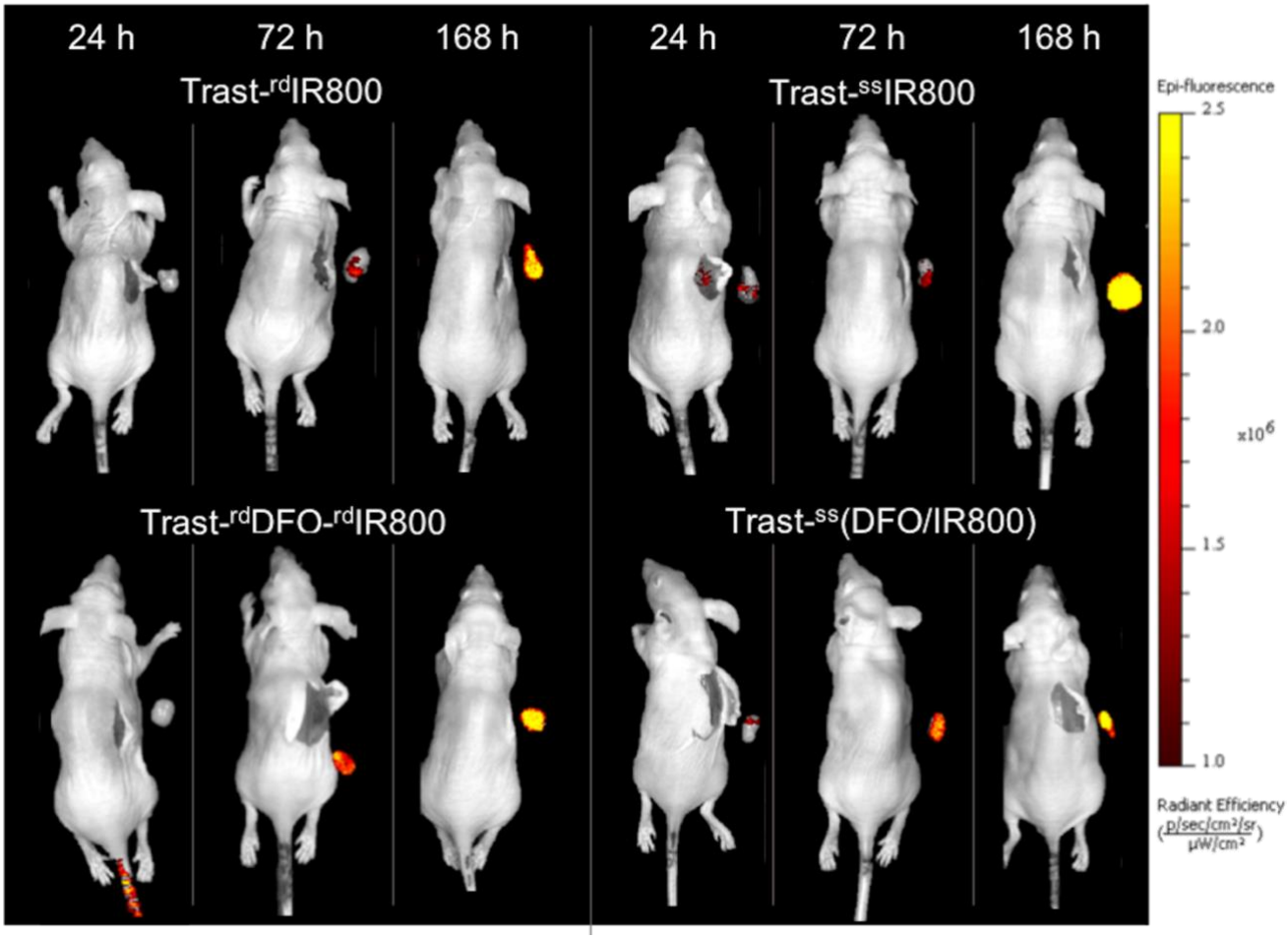

Figure 7. In vivo fluorescence images of mice xenografted with HER2+ SKOV-3 cells, after injection of trast-rdIR800, trast-^{ss}IR800, [^{89}Zr]Zr-trast-rdDFO-rdIR800, [^{89}Zr]Zr-trast-^{ss}(DFO/IR800) after tumor dissection (tumors on right side of mice). After resection, tumor was placed on the side of the mouse. Representative mice injected with [^{89}Zr]Zr-trast-rdDFO-rdIR800, [^{89}Zr]Zr-trast-^{ss}(DFO/IR800) (n=5/group), trast-rdIR800 and trast-^{ss}IR800 are depicted (n=3/group)

CONCLUSION

The strategy at hand is a significant improvement over the current clinical standard (dual-random conjugate). First of all, the strategy developed in this study allows to control easily and efficiently the conjugation site, the degree of labeling of both chelator and fluorophore, and the ratio of these reporters. The site-specific MOMIP strategy dramatically improved the resistance of the fluorophore to radiobleaching, both in PBS and in serum. Finally, the site-specific conjugation method used for the grafting of the MOMIP allowed to reduce the non-specific uptake in the spleen and liver. This is particularly important for the latter, as it mitigates the dramatic increase of liver uptake caused by adjunction of a fluorophore.

However, there is still room for improvement. The major drawback of this new conjugate is certainly the increased ^{89}Zr release observed *in vivo* and to a lesser extend *in vitro*, which have translated in a significantly higher bone uptake at early time points. Although this specific behavior seemed to fade over time, it is important that we understand the mechanism at play here. Furthermore, reaching high A_s proved challenging with our site-specific bimodal conjugate. In order to improve these points and better comprehend the phenomenon, we are planning in future studies to adjust the structure of our MOMIP by adding a PEG spacer, drawing away the chelator in order to reduce the likely steric hindrance caused by the proximity of the fluorophore. A second line of investigation for improving the *in vivo*

behavior of our site-specific bimodal conjugate would be to switch gear and use recently developed chelators known to form more stable Zr^{4+}-complexes than the standard DFO used in this work,[29,43,44] therefore reducing Zr release and bone uptake.
It is important to note that the strategy applied above is not limited to trastuzumab or the imaging reporters used in this study. The conjugation strategy can be applied to a wide range of IgGs (all glycan-bearing mAbs - mAb produced by mammalian cells), and the synthetic route of the MOMIP is based on a highly versatile and easily accessible scaffold which could be quickly adapted to other imaging reporters. These points make this conjugation strategy highly modular for the dual labeling of immunoconjugates.
Finally, we would like to emphasize that trastuzumab is notorious for its robustness and imperviousness to random conjugation, with the majority (≈ 80 %) of conjugated lysines located in the constant region,[45] which reduces the likeliness of interfering with antigen binding. Consequently, we believe that the conclusions drawn from the present study are very likely to have even more dramatic consequences on less sturdy antibodies.

MATERIAL AND METHODS

A detailed description of experimental procedures — including synthetic protocols, bioconjugation techniques, radiolabeling methodologies, and the design and execution of *in vitro* and *in vivo* experiments — can be found in the Supplementary Information (see SI).

ACKNOWLEDGMENTS

Funding sources

This study received funding from the Innovative Medicines Initiative 2 Joint Undertaking under grant agreement No 116106. This Joint Undertaking received support from the European Union's Horizon 2020 research and innovation program and EFPIA. In addition, this work was supported by the Centre National de la Recherche Scientifique (CNRS), the Université de Bourgogne, the Conseil Régional de Bourgogne Franche-Comté through the « Plan d'Action Régional pour l'Innovation » (program PARI) and by the European Union through the PO FEDER-FSE 2014/2020 Bourgogne program.

Acknowledgements

The authors thank the "Plateforme d'Analyse Chimique et de Synthèse Moléculaire de l'Université de Bourgogne" (PACSMUB, http://www.wpcm.fr) for access to analytical instrumentation, and Marie-José Penouilh (University of Burgundy, PACSMUB) and Dr. Quentin Bonnin (University of Burgundy, PACSMUB) for the high-resolution mass spectrometry.

SUPPORTING INFORMATION DESCRIPTION

Materials and methods, experimental details on chemical synthesis, immunoconjugation, *in vitro* stability, affinity assays and *in vivo* behavior. Additional figures for the immunoconjugates mass spectrometry, immunoreactivity, in vitro stability, radiobleaching and in vivo behavior (blood kinetics and MIP images). Additional tables on the DOL of the conjugates, experimental set up for PET imaging and *ex vivo* biodistribution data.

ABBREVIATIONS

BCN: (1R,8S,9S)-bicyclo[6.1.0]non-4-yne; DFO: desferrioxamine B; DOL: degree of labeling; EDTA: ethylenediaminetetraacetic acid; IC_{50}: half-maximal inhibitory concentration; IgG: immunoglobulin G; mAb: monoclonal antibody; MOMIP: monomolecular multimodal imaging probe; NIRF: near-infrared fluorescence; PBS: phosphate buffer saline; PET: positron emission tomography; RCY: radiochemical yield; A_s:

specific activity; SPAAC: strain-promoted alkyne-azide cycloaddition; SPECT: single-photon emission computed tomography.

REFERENCES

1. Hernot S, Manen L van, Debie P, Mieog JSD & Vahrmeijer AL. Latest developments in molecular tracers for fluorescence image-guided cancer surgery. The Lancet Oncology. 2019; 20: e354–e367. DOI: 10.1016/S1470-2045(19)30317-1.
2. Azhdarinia A, Ghosh P, Ghosh S, Wilganowski N & Sevick-Muraca EM. Dual-Labeling Strategies for Nuclear and Fluorescence Molecular Imaging: A Review and Analysis. Mol Imaging Biol. 2012; 14: 261–276. DOI: 10.1007/s11307-011-0528-9.
3. Thorp-Greenwood FL & Coogan MP. Multimodal radio- (PET/SPECT) and fluorescence imaging agents based on metallo-radioisotopes: current applications and prospects for development of new agents. Dalton Trans. 2011; 40: 6129–6143. DOI: 10.1039/C0DT01398F.
4. Seibold U, Wängler B, Schirrmacher R & Wängler C. Bimodal Imaging Probes for Combined PET and OI: Recent Developments and Future Directions for Hybrid Agent Development. Biomed Res. Int. 2014; 2014:153741. doi:10.1155/2014/153741DOI: 10.1155/2014/153741.
5. Singh G, Gott MD, Pietzsch H-J & Stephan H. Nuclear and optical dual-labelled imaging agents. Design and challenges. Nuklearmedizin. 2016; 55: 41–50.
6. Zhao J, Chen J, Ma S, Liu Q, Huang L, Chen X, Lou K & Wang W. Recent developments in multimodality fluorescence imaging probes. Acta Pharmaceutica Sinica B. 2018; 8: 320–338. DOI: 10.1016/j.apsb.2018.03.010.
7. Hendricks JA, Keliher EJ, Wan D, Hilderbrand SA, Weissleder R & Mazitschek R. Synthesis of [18F]BODIPY: Bifunctional Reporter for Hybrid Optical/Positron Emission Tomography Imaging. Angewandte Chemie International Edition. 2012; 51: 4603–4606. DOI: 10.1002/anie.201107957.

8. Ono M, Watanabe H, Ikehata Y, Ding N, Yoshimura M, Sano K & Saji H. Radioiodination of BODIPY and its application to a nuclear and optical dual functional labeling agent for proteins and peptides. Scientific Reports. 2017; 7: 3337. DOI: 10.1038/s41598-017-03419-z.
9. Ariztia J, Solmont K, Moïse NP, Specklin S, Heck MP, Lamandé-Langle S & Kuhnast B. PET/Fluorescence Imaging: An Overview of the Chemical Strategies to Build Dual Imaging Tools. Bioconjugate Chem. 2022; 33: 24–52. DOI: 10.1021/acs.bioconjchem.1c00503.
10. Hekman MC, Rijpkema M, Muselaers CH, Oosterwijk E, Hulsbergen-Van de Kaa CA, Boerman OC, Oyen WJ, Langenhuijsen JF & Mulders PF. Tumor-targeted Dual-modality Imaging to Improve Intraoperative Visualization of Clear Cell Renal Cell Carcinoma: A First in Man Study. Theranostics. 2018; 8: 2161–2170. DOI: 10.7150/thno.23335.
11. Clinical trial 'Multi-modality Imaging in Peritoneal Carcinomatosis of Colorectal'. ClinicalTrials.gov Identifier: NCT03699332.
12. Kristensen LK, Christensen C, Jensen MM, Agnew BJ, Schjöth-Frydendahl C, Kjaer A & Nielsen CH. Site-specifically labeled ^{89} Zr-DFO-trastuzumab improves immuno-reactivity and tumor uptake for immuno-PET in a subcutaneous HER2-positive xenograft mouse model. Theranostics. 2019; 9: 4409–4420. DOI: 10.7150/thno.32883.
13. Xu H, Baidoo K, Gunn AJ, Boswell CA, Milenic DE, Choyke PL & Brechbiel MW. Design, Synthesis, and Characterization of a Dual Modality Positron Emission Tomography and Fluorescence Imaging Agent for Monoclonal Antibody Tumor-Targeted Imaging. J. Med. Chem. 2007; 50: 4759–4765. DOI: 10.1021/jm070657w.
14. Xu H, Eck PK, Baidoo KE, Choyke PL & Brechbiel MW. Toward preparation of antibody-based imaging probe libraries for dual-modality positron emission tomography

and fluorescence imaging. Bioorg. Med. Chem. 2009; 17: 5176–5181. DOI: 10.1016/j.bmc.2009.05.048.

15. Maindron N, Ipuy M, Bernhard C, Lhenry D, Moreau M, Carme S, Oudot A, Collin B, Vrigneaud J-M, Provent P, *et al.* Near-Infrared-Emitting BODIPY-trisDOTA(111)In as a Monomolecular Multifunctional Imaging Probe: From Synthesis to In Vivo Investigations. Chem. Eur. J. 2016; 22: 12670–12674. DOI: 10.1002/chem.201602886.
16. Meimetis LG, Boros E, Carlson JC, Ran C, Caravan P & Weissleder R. Bioorthogonal Fluorophore Linked DFO—Technology Enabling Facile Chelator Quantification and Multimodal Imaging of Antibodies. Bioconjugate Chem. 2016; 27: 257–263. DOI: 10.1021/acs.bioconjchem.5b00630.
17. Rodriguez EA, Wang Y, Crisp JL, Vera DR, Tsien RY & Ting R. New Dioxaborolane Chemistry Enables [18F]-Positron-Emitting, Fluorescent [18F]-Multimodality Biomolecule Generation from the Solid Phase. Bioconjugate Chem. 2016; 27: 1390–1399. DOI: 10.1021/acs.bioconjchem.6b00164.
18. Adams CJ, Wilson JJ & Boros E. Multifunctional Desferrichrome Analogues as Versatile 89Zr(IV) Chelators for ImmunoPET Probe Development. Mol. Pharmaceutics. 2017; 14: 2831–2842. DOI: 10.1021/acs.molpharmaceut.7b00343.
19. Lu Z, Pham TT, Rajkumar V, Yu Z, Pedley RB, Årstad E, Maher J & Yan R. A Dual Reporter Iodinated Labeling Reagent for Cancer Positron Emission Tomography Imaging and Fluorescence-Guided Surgery. J. Med. Chem. 2018; 61: 1636–1645. DOI: 10.1021/acs.jmedchem.7b01746.
20. Ahn SH, Thach D, Vaughn BA, Alford VM, Preston AN, Laughlin ST & Boros E. Linear Desferrichrome-Linked Silicon–Rhodamine Antibody Conjugate Enables Targeted Multimodal Imaging of HER2 in Vitro and in Vivo. Mol. Pharmaceutics. 2019; 16: 1412–1420. DOI: 10.1021/acs.molpharmaceut.8b01278.

21. Canovas C, Moreau M, Vrigneaud J-M, Bellaye P-S, Collin B, Denat F & Goncalves V. Modular Assembly of Multimodal Imaging Agents through an Inverse Electron Demand Diels–Alder Reaction. Bioconjugate Chem. 2019; 30: 888–897. DOI: 10.1021/acs.bioconjchem.9b00017.
22. Adumeau P, Carnazza KE, Brand C, Carlin SD, Reiner T, Agnew BJ, Lewis JS & Zeglis BM. A Pretargeted Approach for the Multimodal PET/NIRF Imaging of Colorectal Cancer. Theranostics. 2016; 6: 2267–2277. DOI: 10.7150/thno.16744.
23. Tsai WK, Zettlitz KA, Tavaré R, Kobayashi N, Reiter RE & Wu AM. Dual-Modality ImmunoPET/Fluorescence Imaging of Prostate Cancer with an Anti-PSCA Cys-Minibody. Theranostics. 2018; 8: 5903–5914. DOI: 10.7150/thno.27679.
24. Zettlitz KA, Tsai W-TK, Knowles SM, Kobayashi N, Donahue TR, Reiter RE & Wu AM. Dual-Modality Immuno-PET and Near-Infrared Fluorescence Imaging of Pancreatic Cancer Using an Anti–Prostate Stem Cell Antigen Cys-Diabody. J. Nucl. Med. 2018; 59: 1398–1405. DOI: 10.2967/jnumed.117.207332.
25. Houghton JL, Zeglis BM, Abdel-Atti D, Aggeler R, Sawada R, Agnew BJ, Scholz WW & Lewis JS. Site-specifically labeled CA19.9-targeted immunoconjugates for the PET, NIRF, and multimodal PET/NIRF imaging of pancreatic cancer. PNAS. 2015; 112: 15850–15855. DOI: 10.1073/pnas.1506542112.
26. Spycher PR, Amann CA, Wehrmüller JE, Hurwitz DR, Kreis O, Messmer D, Ritler A, Küchler A, Blanc A, Béhé M, *et al.* Dual, Site-Specific Modification of Antibodies by Using Solid-Phase Immobilized Microbial Transglutaminase. ChemBioChem. 2017; 18: 1923–1927. DOI: 10.1002/cbic.201700188.
27. Wang Y, Miao Z, Ren G, Xu Y & Cheng Z. A novel Affibody bioconjugate for dual-modality imaging of ovarian cancer. Chem. Commun. 2014; 50: 12832–12835. DOI: 10.1039/C4CC03454F.

28. Canovas C, Moreau M, Bernhard C, Oudot A, Guillemin M, Denat F & Goncalves V. Site-Specific Dual Labeling of Proteins on Cysteine Residues with Chlorotetrazines. Angewandte Chemie International Edition. 2018; 57: 10646–10650. DOI: 10.1002/anie.201806053.
29. Heskamp S, Raavé R, Boerman O, Rijpkema M, Goncalves V & Denat F. 89Zr-Immuno-Positron Emission Tomography in Oncology: State-of-the-Art 89Zr Radiochemistry. Bioconjugate Chem. 2017; 28: 2211–2223. DOI: 10.1021/acs.bioconjchem.7b00325.
30. Adumeau P, Sharma SK, Brent C & Zeglis BM. Site-Specifically Labeled Immunoconjugates for Molecular Imaging--Part 1: Cysteine Residues and Glycans. Mol. Imaging Biol. 2016; 18: 1–17. DOI: 10.1007/s11307-015-0919-4.
31. van Geel R, Wijdeven MA, Heesbeen R, Verkade JMM, Wasiel AA, van Berkel SS & van Delft FL. Chemoenzymatic Conjugation of Toxic Payloads to the Globally Conserved N-Glycan of Native mAbs Provides Homogeneous and Highly Efficacious Antibody–Drug Conjugates. Bioconjugate Chem. 2015; 26: 2233–2242. DOI: 10.1021/acs.bioconjchem.5b00224.
32. Bunschoten A, Buckle T, Visser NL, Kuil J, Yuan H, Josephson L, Vahrmeijer AL & van Leeuwen FWB. Multimodal interventional molecular imaging of tumor margins and distant metastases by targeting αvβ3 integrin. Chembiochem. 2012; 13: 1039–1045. DOI: 10.1002/cbic.201200034.
33. Li D, Zhang J, Chi C, Xiao X, Wang J, Lang L, Ali I, Niu G, Zhang L, Tian J, *et al.* First-in-human study of PET and optical dual-modality image-guided surgery in glioblastoma using ^{68}Ga-IRDye800CW-BBN. Theranostics. 2018; 8: 2508–2520. DOI: 10.7150/thno.25599.
34. Debie P, Declerck NB, van Willigen D, Huygen CM, De Sloovere B, Mateusiak L, Bridoux J, Puttemans J, Devoogdt N, van Leeuwen FWB, *et al.* The Design and

Preclinical Evaluation of a Single-Label Bimodal Nanobody Tracer for Image-Guided Surgery. Biomolecules. 2021; 11: 360. DOI: 10.3390/biom11030360.

35. Sharma SK, Glaser JM, Edwards KJ, Khozeimeh Sarbisheh E, Salih AK, Lewis JS & Price EW. A Systematic Evaluation of Antibody Modification and 89Zr-Radiolabeling for Optimized Immuno-PET. Bioconjugate Chem. 2020; doi:10.1021/acs.bioconjchem.0c00087DOI: 10.1021/acs.bioconjchem.0c00087.
36. Hernandez R, Heskamp S, Rijpkema M, Bos DL, Goldenberg DM, McBride WJ, Morgenstern A, Bruchertseifer F, Cai W & Boerman OC. Preventing Radiobleaching of Cyanine Fluorophores Enhances Stability of Nuclear/NIRF Multimodality Imaging Agents. Theranostics. 2017; 7: 1–8. DOI: 10.7150/thno.15124.
37. Motchnik PA, Frei B & Ames BN. Measurement of antioxidants in human blood plasma. Meth. Enzymol. 1994; 234: 269–279. DOI: 10.1016/0076-6879(94)34094-3.
38. Vivier D, Sharma SK, Adumeau P, Rodriguez C, Fung K & Zeglis BM. The Impact of FcγRI Binding on Immuno-PET. J. Nucl. Med. 2019; 60: 1174–1182. DOI: 10.2967/jnumed.118.223636.
39. Vivier D, Fung K, Rodriguez C, Adumeau P, Ulaner GA, Lewis JS, Sharma SK & Zeglis BM. The Influence of Glycans-Specific Bioconjugation on the FcγRI Binding and *In vivo* Performance of ^{89} Zr-DFO-Pertuzumab. Theranostics. 2020; 10: 1746–1757. DOI: 10.7150/thno.39089.
40. Cohen R, Stammes MA, de Roos IH, Stigter-van Walsum M, Visser GW & van Dongen GA. Inert coupling of IRDye800CW to monoclonal antibodies for clinical optical imaging of tumor targets. EJNMMI Res. 2011; 1: 31. DOI: 10.1186/2191-219X-1-31.
41. Cohen R, Vugts DJ, Stigter-van Walsum M, Visser GWM & van Dongen GAMS. Inert coupling of IRDye800CW and zirconium-89 to monoclonal antibodies for single- or dual-

mode fluorescence and PET imaging. Nat Protoc. 2013; 8: 1010–1018. DOI: 10.1038/nprot.2013.054.

42. Debie P, Van Quathem J, Hansen I, Bala G, Massa S, Devoogdt N, Xavier C & Hernot S. Effect of Dye and Conjugation Chemistry on the Biodistribution Profile of Near-Infrared-Labeled Nanobodies as Tracers for Image-Guided Surgery. Mol. Pharmaceutics. 2017; 14: 1145–1153. DOI: 10.1021/acs.molpharmaceut.6b01053.
43. Bhatt NB, Pandya DN & Wadas TJ. Recent Advances in Zirconium-89 Chelator Development. Molecules. 2018; 23: 638. DOI: 10.3390/molecules23030638.
44. Raavé R, Sandker G, Adumeau P, Jacobsen CB, Mangin F, Meyer M, Moreau M, Bernhard C, Da Costa L, Dubois A, *et al.* Direct comparison of the in vitro and in vivo stability of DFO, DFO* and DFOcyclo* for 89Zr-immunoPET. Eur J Nucl Med Mol Imaging. 2019; 46: 1966–1977. DOI: 10.1007/s00259-019-04343-2.
45. Chen L, Wang L, Shion H, Yu C, Yu YQ, Zhu L, Li M, Chen W & Gao K. In-depth structural characterization of Kadcyla® (ado-trastuzumab emtansine) and its biosimilar candidate. MAbs. 2016; 8: 1210–1223. DOI: 10.1080/19420862.2016.1204502.

TABLE OF CONTENTS